Electronic Supplementary Information

Reactivity trends of the $MoVO_x$ mixed metal oxide catalyst from density functional modeling†

Wen-Qing Li,[‡a] Torstein Fjermestad,[‡a] Alexander Genest,[a] Notker Rösch*[ab]

[a] Institute of High Performance Computing, Agency for Science, Technology and Research, 1 Fusionopolis Way, #16-6 Connexis, Singapore 138632

[b] Department Chemie and Catalysis Research Center, Technische Universität München, 85747 Garching, Germany, *E-mail: roesch@mytum.de

‡ W.-Q. L. and T. F. contributed equally to this work.

Table of Contents

S1. Computational details

All electronic structure calculations were carried out using density-functional theory (DFT) as implemented in the code CRYSTAL14.[1] To ensure an adequate representation of the energetics of the oxidation reactions and a proper localization of the reducing electrons,[2-4] we selected the hybrid DFT method B3LYP[5] in the unrestricted Kohn-Sham variant. We chose to add the empirical dispersion the D2 correction.[6] Orbitals were represented with the help of the Gaussian-type split-valence basis sets: 86-411d31G for V,[7] 8-411d1 for O,[8] and 5-11G* for H.[9] For Mo we selected the Hay-Wadt small-core effective core potential,[10] in combination with the 311(d31)G basis set for valence electrons.[11] The integrations over the Brillouin zone were carried out using 1×1×1 grids.[12] We set the threshold parameters ITOL1 to ITOL5, that control the evaluation of Coulomb and exchange integrals[13] to 7, 7, 7, 9, and 30, respectively, and the SCF convergence criterion to 10^{-7} a.u. Geometry optimizations were considered converged when (*i*) the root mean square (RMS) value of the atomic displacements was below 1.2×10^{-3} a.u. and the largest value of the atomic displacements below 1.8×10^{-3} a.u; (*ii*) the RMS of the atomic energy gradients was below 3.0×10^{-4} a.u. and the corresponding largest value below 4.5×10^{-4} a.u. For the unit cell, we selected the idealized stoichiometry $Mo_{30}V_{10}O_{112}$.

For the adsorption of a water molecule and the hydrolyzed structures of slab model **II**, we probed the size of the basis set superposition error by evaluating counterpoise corrections.[14] These corrections amounted to 19 kJ mol^{-1} for the adsorption energy of H_2O and to 26–31 kJ mol^{-1} for the reaction energy of the hydrolysis processes. Due to the similar nature of the environment for both slab models **I** and **II**, we assume~~d~~ only minor changes in these corrections for slab model **I**.

The vibrational corrections to the free energy for the H_2O adsorption was calculated with the software VASP, version 5.4.4[15, 16], including VTST additions.[17] We used the projector augmented-wave (PAW) method[18, 19] to treat the core electrons. The 12 valence electrons for Mo, 11 for V, and 6 for O were modeled using a plane-wave representation with a cutoff energy of 400 eV. We employed the PBE exchange-correlation functional[20, 21] and augmented it by a U term, PBE+U.[22] We tested a U value of 3.9 eV and applied it for describing the localization of unpaired electrons in the 3*d* and 4*d* orbitals of Mo and V. We utilized a characteristic parameter of 0.05 eV for a Gaussian level broadening technique[23] and extrapolated the total energy to zero broadening. To obtain an adequate accuracy of the normal modes, we first re-optimized the geometry using VASP, setting the SCF convergence to 10^{-8} eV and the convergence threshold criterion in the geometry optimization to 0.01 eV/Å for the energy gradient of each atom. The normal modes were determined by the dynamical matrix method

provided within the VTST tools set.[17]

In the *c* direction, above the top layer, we added an interlayer spacing of 1.5 nm between the 3L slabs to avoid interactions between a slab and its images. For the integration over the Brillouin zone we restricted the *k*-grid to the Γ-point. The normal-mode analysis included the adsorbate and the top layer of the 3L slab. For estimating Gibbs free energies, we accounted only for the vibrational degrees of freedom of the adsorbed species. For the water molecule in the gas phase, we calculated the free energy corrections, including rotation and translation, using the program Gaussian 09.[24]

S2. Statistical model

To quantify how structural and electronic features affect the oxidative dehydrogenation (ODH) and the hydrolysis, we constructed a statistical model. For this purpose, we defined 8 predictor variables, grouped into two categories: (*i*) the location of the proton and (*ii*) the location of the polarons in the pentameric unit, see Figure 2 of the main text. In both the hydrogenation and hydrolysis reactions, the proton can adsorb at the O sites **tm**, **br1**, **br2**, **br3**, Figure 2 of the main text. We specified, whether a proton is adsorbed or not on these sites, by assigning the values 1 or 0, respectively. In the hydrogenations, the polarons of the pentameric unit may be located at the metal sites **4b**, **7b$_M$**, **7a**, and **7b**; in the hydrolysis, they are located only on the sites **7a** and **7b**. Similarly, as in the case of the H adsorption, we assigned values 1 or 0 to the variables indicating whether or not a polaron is located at these centers. To the resulting linear model, we applied a partial least squares regression procedure.[25, 26]

We used the structures with the polaron located at sites **7b** or **7b$_M$** for slab model **I** and at sites **4b** and **7b$_M$** for slab model **II**, 16 structures in total. We fitted the data invoking three components in the partial least squares regression procedure. We assessed the error with the leave-one-out cross validation,[27-29] which leaves one data point out of the fit and determines the error of this data point. Doing so for each data point in turn, we calculated a root mean square error of prediction (RMSEP) of 12.2 kJ mol^{-1}. The resulting regression coefficients are given in Table S2. The calculations were calculated in the statistics framework R.[30]

S3. Tables

Table S1. Energies E (kJ mol^{-1}) of slab models **I** to **IV**, relative to slab **I**.

Slab model	**I**	**II**	**III**	**IV**
E	0	18	47	80

Table S2. Regression coefficients (energy contributions C) of the linear model for E_r(ODH) as a function of the proton adsorption sites and the polaron locations. Values in kJ mol^{-1}.

H site	C	Polaron location	C
tm	47.64	**4b**	45.33
br1	-1.41	**7a**	-10.93
br2	-19.99	**7b**	-12.95
br3	-26.24	**7b$_M$**	-35.22

Table S3. Hydrogen adsorption energies E_{ads} calculated for the proton at the sites **tm**, **br1**, **br2**, or **br3**. BEP estimates E_a of the corresponding reaction barriers; see text for details. The newly created polaron is located at sites **2a**, **4b**, **7b**, or **7b$_M$**. Energies in kJ mol^{-1}.

	E_{ads}						E_a	
Slab model	**I**			**II**			**I**	**II**
	4b	**7b**	**7b$_M$**	**2a**	**4b**	**7b$_M$**	**7b**	**4b**
tm		-286	-311	-260	-248	-336		
br1	-312	-337	-364		-307	-371	125	142
br2		-363	-381		-313	-396		139
br3		-360	-370		-331	-418	110	

Table S4. Energy differences of the initial H adsorption of ODH and the hydrolysis (Hydr.) between pairs of reactions involving H in the final state at the sites **tm**/**br1, br1**/**br2, br2/br3**, calculated for slab models **I** and **II**. MAD is the mean absolute deviation evaluated for each pair of H sites at a given slab model. Also given is the site of the newly created polaron (ODH) or the initial site of H_2O adsorption (hydrolysis). Energies in kJ mol^{-1}.

Slab model	**I**				**II**			
	ODH		Hydr.	MAD	ODH		Hydr.	MAD
	7b	**7b$_M$**	**4b**		**4b**	**7b$_M$**	**4b**	
tm/**br1**	-51	-53	-61	4	-59	-34	-40	10
br1/**br2**	-26	-18	-12	5	-6	-26	-16	7
br2/**br3**	2	11	4	4	-17	-21	-18	2

Table S5. Calculated reaction energies E_r of water adsorption (H_2O) or hydrolysis (H), i.e., the energy for transferring the adsorbate (Ads.) to the specified site, on the $MoVO_x$ surface, represented by slab models **I** and **II**. The reference energy for H_2O adsorption and the hydrolysis is the bare slab model and an H_2O molecule at infinite separation. The counterpoise corrected energies E_{rCP} given for selected processes. Free energy values G_r computed for the intermediate and final states of the most favorable hydrolysis process. Energies in kJ mol^{-1}.

Slab	model	**I**	**II**			
Ads.	site	E_r	E_r	E_{rCP}	G_r[a]	G_r[b]
H_2O	**7b**	-68	-84			
	4b	-98	-106	-87	-31	-4
H[c]	**tm**	17	-16	11		
	br1	-44	-56	-27		
	Br2	-56	-72	-41		
	br3	-52	-90	-63	-7	22

[a] Evaluated at 298 K. [b] Evaluated at 488 K. [c] OH is adsorbed at site **4b**.

S4. Figures

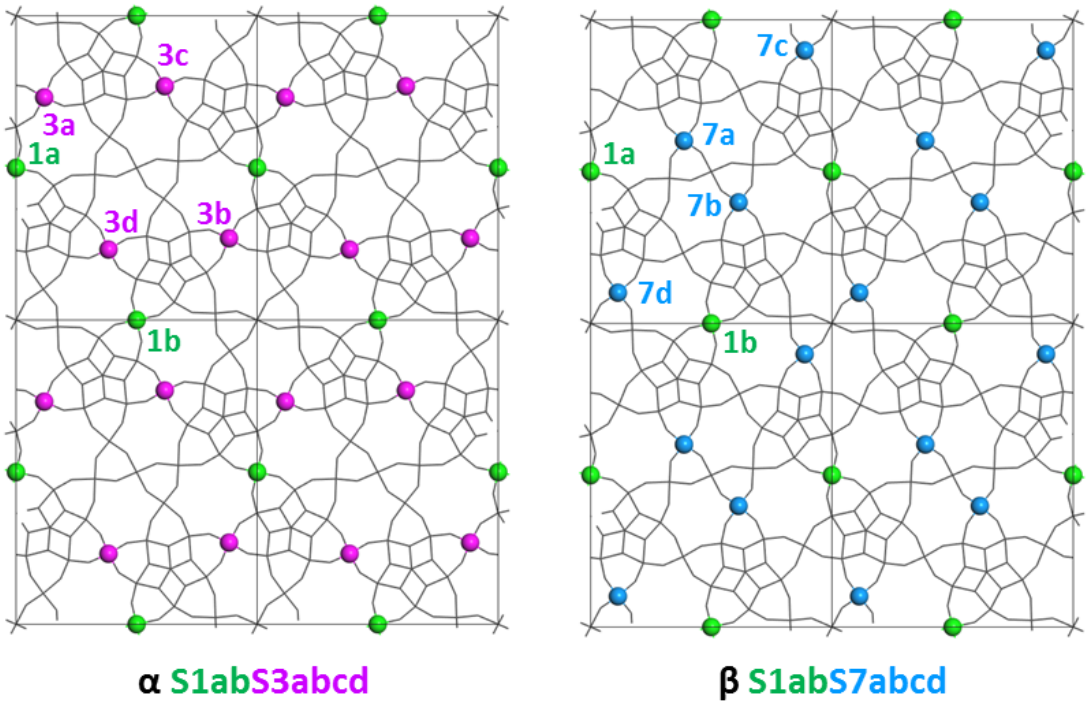

Figure S1. Bulk structures α (left) and β (right) used for constructing the slab models **I** to **IV**. Color coding of the metal centers: green – S1; pink – S3; light blue – S7.

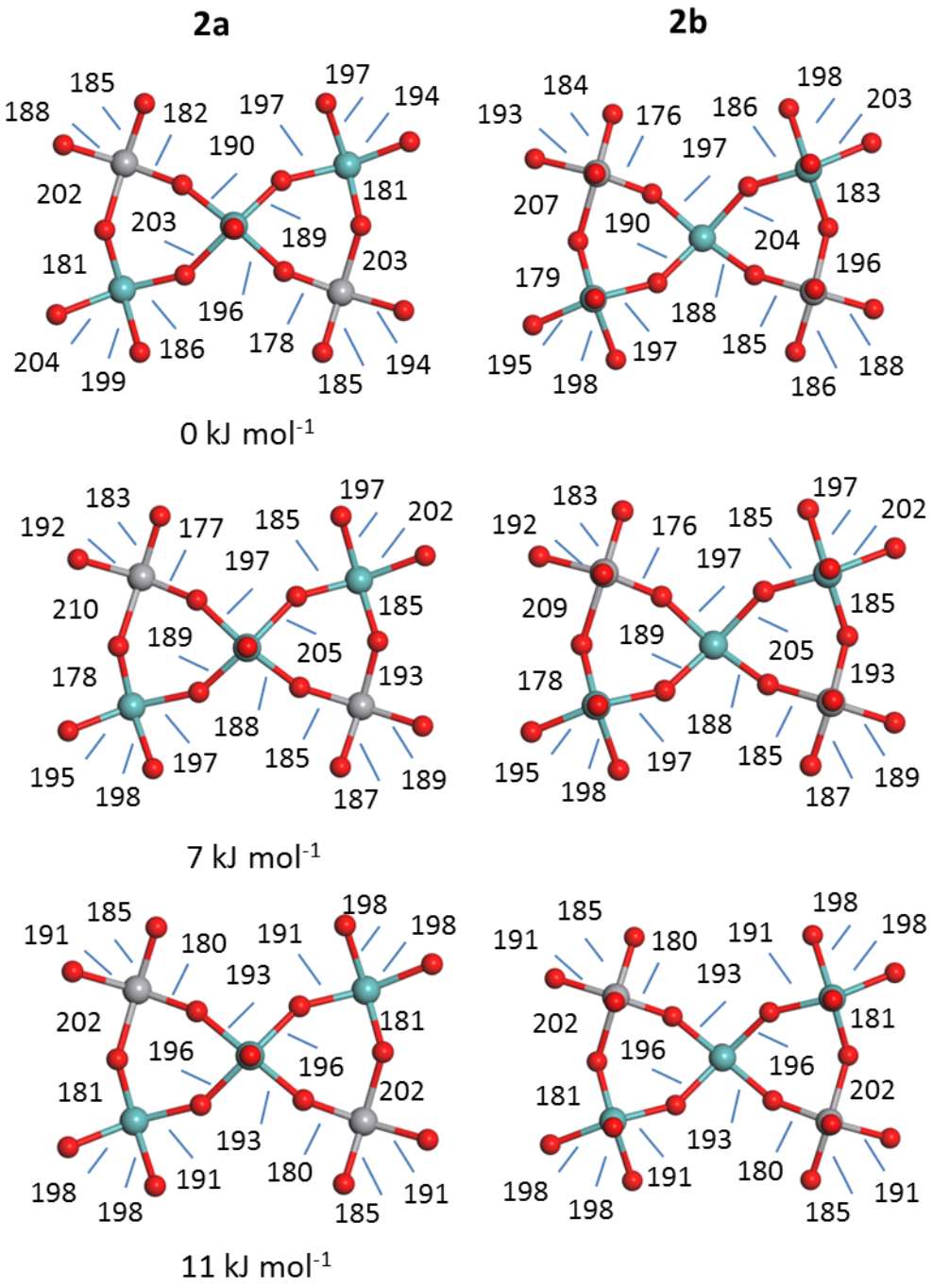

Figure S2. Three isomers of slab model **I** showing both pentameric units around centers **2a** and **2b**. Distances in pm. Colors coding: V – grey, Mo – teal, O – red.

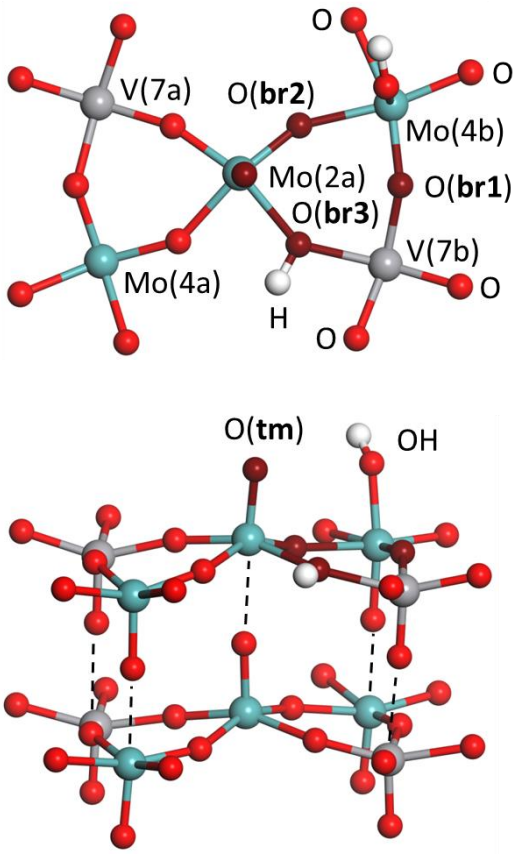

Figure S3. Active sites of hydrolysis. Specifically shown for the final state of the hydroloysis process **br3.II**. Upper panel – top view, lower panel – side view. Color coding as in Figure S2; in addition: H – white, O at adsorption sites – dark red.

References

1. R. Dovesi, R. Orlando, A. Erba, C. M. Zicovich-Wilson, B. Civalleri, S. Casassa, L. Maschio, M. Ferrabone, M. De La Pierre and P. D'Arco, *Int. J. Quantum Chem.*, 2014, **114**, 1287-1317.
2. A. J. Cohen, P. Mori-Sánchez and W. Yang, *Science*, 2008, **321**, 792-794.
3. P. Mori-Sánchez, A. J. Cohen and W. Yang, *Phys. Rev. Lett.*, 2008, **100**, 146401.
4. A. J. Cohen, P. Mori-Sánchez and W. Yang, *Chem. Rev.*, 2011, **112**, 289-320.
5. A. D. Becke, *J. Chem. Phys.*, 1993, **98**, 5648-5652.
6. S. Grimme, *J. Comput. Chem.*, 2006, **27** 1787-1799.
7. E. Ruiz, M. Llunell and P. Alemany, *J. Solid State Chem.*, 2003, **176**, 400-411.
8. T. Bredow, K. Jug and R. A. Evarestov, *Phys. Status Solidi B*, 2006, **243**, R10–R12.
9. R. Dovesi, C. Ermondi, E. Ferrero, C. Pisani and C. Roetti, *Phys. Rev. B*, 1984, **29**, 3591.
10. P. J. Hay and W. R. Wadt, *J. Chem. Phys.*, 1985, **82**, 270-283.
11. F. Cora, A. Patel, N. M. Harrison, C. Roetti and C. Richard A. Catlow, *J. Mater. Chem.*, 1997, **7**, 959-967.
12. H. J. Monkhorst and J. D. Pack, *Phys. Rev. B*, 1976, **13**, 5188.
13. R. Dovesi, V. R. Saunders, C. Roetti, R. Orlando, C. M. Zicovich-Wilson, F. Pascale, B. Civalleri, K. Doll, N. M. Harrison, I. J. Bush, P. D'Arco, M. Llunell, M. Causà and Y. Noël, *CRYSTAL14 User's Manual.*, University of Torino, Torino, 2014.
14. C. J. Cramer, *Essentials of Computational Chemistry Theories and Models*, John Wiley & Sons, Ltd., Chichester, West Sussex, England, 2004.
15. G. Kresse and J. Hafner, *Phys. Rev. B*, 1994, **49**, 14251-14269.
16. G. Kresse and J. Furthmüller, *Comput. Mat. Sci.*, 1996, **6**, 15-50.
17. *VTSTTools 3.1*, University of Texas, Austin, 2018.
18. P. E. Blöchl, *Phys. Rev. B*, 1994, **50**, 17953.
19. G. Kresse and D. Joubert, *Phys. Rev. B*, 1999, **59**, 1758-1775.
20. J. P. Perdew, K. Burke and M. Ernzerhof, *Phys. Rev. Lett.*, 1996, **77**, 3865-3868.
21. J. P. Perdew, K. Burke and M. Ernzerhof, *Phys. Rev. Lett.*, 1997, **78**, 1396.
22. S. L. Dudarev, G. A. Botton, S. Y. Savrasov, C. J. Humphreys and A. P. Sutton, *Phys. Rev. B*, 1998, **57**, 1505-1509
23. G. Kresse, M. Marsman, J. Furthmüller, *VASP Manual*, Universität Wien, Vienna, 2016.
24. M. Frisch, G. Trucks, H. B. Schlegel, G. E. Scuseria, M. A. Robb, J. R. Cheeseman, G. Scalmani, V. Barone, B. Mennucci and G. Petersson, *Inc., Wallingford, CT*, 2009.
25. S. Wold, M. Sjöström and L. Eriksson, *Chemom. Intell. Lab. Syst.*, 2001, **58**, 109-130.
26. P. Geladi and B. R. Kowalski, *Anal. Chim. Acta*, 1986, **185**, 1-17.
27. D. M. Allen, *Technometrics*, 1974, **16**, 125-127.
28. M. Stone, *J. R. Stat. Soc. Series B Stat. Methodol.*, 1974, **36**, 111-147.
29. S. Geisser, *J Am Stat Assoc.*, 1975, **70**, 320-328.
30. R. Wehrens and B.-H. Mevik, *J. Stat. Softw.*, 2007, **18**, 1-23.